Author Manuscript

Author Manuscript

Author Manuscript

Author Manuscript

HHS Public Access

Author manuscript

Nat Immunol. Author manuscript; available in PMC 2011 April 01.

Published in final edited form as:

Nat Immunol. 2010 October ; 11(10): 953–961. doi:10.1038/ni.1936.

Confinement-Optimized 3-Dimensional T cell Amoeboid Motility is Modulated via Myosin IIA-Regulated Adhesions

Jordan Jacobelli[1], **Rachel S. Friedman**[1], **Mary Anne Conti**[2], **Ana-Maria Lennon-Dumenil**[3], **Matthieu Piel**[3], **Caitlin M. Sorensen**[1], **Robert S. Adelstein**[2], and **Matthew F. Krummel**[1]

[1]Department of Pathology; University of California San Francisco. 513 Parnassus Avenue HSW-0511, San Francisco CA 94143 USA.

[2]Laboratory of Molecular Cardiology; National Heart, Lung and Blood Institute, NIH, 10 Center Drive MSC-1583, Bethesda, MD 20892, USA.

[3]INSERM U653, Institut Curie, 12 Rue Lhomond, 75005, Paris, France.

Abstract

During trafficking through tissues, T cells fine-tune their motility to balance the extent and duration of cell-surface contacts with the need to traverse an entire organ. *In vivo*, Myosin-IIA-deficient T cells exhibited a triad of defects including over-adherence to high-endothelial venules, reduced interstitial migration, and inefficient completion of recirculation through lymph nodes. Spatiotemporal analysis of 3-dimensional motility in microchannels revealed that the degree of confinement and Myosin-IIA function, rather than integrin adhesion as proposed by the haptokinetic model, optimize motility rate. This occurs via a Myosin-IIA-dependent rapid 'walking' motility mode using multiple small and simultaneous adhesions to the substrate, which prevent spurious and prolonged adhesions. Adhesion discrimination provided by Myosin-IIA is thus necessary for optimizing motility through complex tissues.

Keywords

T cells; Motility; Myosin-IIA; Adhesion; Cytoskeleton

To perform their surveillance functions, T lymphocytes traffic from the vasculature to secondary lymphoid organs where they scan for antigenic peptides on cell surfaces1,2. Within the confinement of these organs, T cells complete a circuit in search of peptide-MHC

Users may view, print, copy, download and text and data- mine the content in such documents, for the purposes of academic research, subject always to the full Conditions of use: http://www.nature.com/authors/editorial_policies/license.html#terms

Correspondence should be addressed to M.F.K. (matthew.krummel@ucsf.edu).

AUTHOR CONTRIBUTIONS

J.J. designed, performed and analyzed all experiments and wrote the manuscript. R.S.F. provided assistance with *in vivo* experiments and participated in 2-photon experiments. M.A.C. and R.S.A. generated the MyoIIA floxed mice and provided reagents. A-M.L-D. and M.P. provided assistance in establishing the microchannel fabrication technique. C.M.S. helped with tissue sectioning and staining, and with mouse typing. M.F.K. coordinated the project, participated in conception and execution of experiments and in writing the manuscript.

AUTHOR DISCLOSURES

The authors declare they have no competing financial interests.

Author Manuscript Author Manuscript Author Manuscript Author Manuscript

bearing antigen-presenting cells (APCs). This task is presumed to involve the competing need to carefully survey every surface while also avoiding excessive adhesion leading to reduced motility. The complex choreography of T cell migration has been observed by 2-photon microscopy3,4; however, the molecular factors coordinating this process are not well understood.

According to the haptokinetic model, in mesenchymal cells, the density of integrin substrate modulates the optimal rate of motility in 2-dimensional (2D) environments5,6. However, it would appear that integrins on their own are not the primary determinant of migration for leukocytes *in vivo* and have been shown to be largely dispensable for amoeboid migration in dense collagen matrices and *in vivo*7–9. As a general rule, protrusion and force generation during motility are mainly mediated by the acto-myosin cytoskeleton through actin polymerization and class-II myosin contraction of the actin network10–12. However, the fundamental mechanisms of this process and the factors that regulate motility, particularly *in vivo*, are yet to be examined.

Amongst the candidates to regulate optimal T cell amoeboid motility in lymphoid tissues, non-muscle Myosin-IIA (MyoIIA) [http://www.signaling-gateway.org/molecule/query?afcsid=A003748] is speculated to play an important role. MyoIIA is the only class II myosin expressed in mouse T lymphocytes and is regulated during T cell arrest mediated by T cell receptor engagement13. In 3-dimensional (3D) collagen matrices, a failure of dendritic cells to ‘squeeze’ through packed collagen fibers was found when myosin-II motor function was blocked7. MyoIIA has also been shown to play an important role in mediating efficient T cell migration *in vitro* in 2D environments13,14. In some model systems, MyoIIA activity is also important in mediating uropodal detachment from highly adhesive surfaces such as ICAM-1 [http://www.signaling-gateway.org/molecule/query?afcsid=A002871] coated substrates15,16.

Previously we have reported that T cells can display two distinct modes of motility in 2D environments, depending on the adhesiveness of the substrate and on MyoIIA activity14. On low adhesive 2D surfaces, T cells display fast amoeboid crawling motility that requires MyoIIA-generated contractile forces and utilizes multiple concurrent surface contacts (‘walking’). In contrast, on high adhesive surfaces, T cell crawling uses a single surface contact, resembles fibroblast and epithelial cell migration, and is mainly driven by actin polymerization (‘sliding’). Our data also indicated that MyoIIA activity restricts surface adhesion on 2D substrates14, but the relevance of this finding to motility within lymph nodes and highly confined environments with numerous possible surface contacts was unclear. The interplay of confinement, provided in 3D environments, and adhesiveness during motility also remains unexplored.

Here we show that MyoIIA function plays a role in multiple steps of T cell trafficking, including interstitial migration of T cells and lymph node retention. Ablation of MyoIIA leads to multiple defects broadly suggesting a generalized lack of cortical control and promiscuous cell-substrate interactions. Using engineered ‘microchannels’ designed to provide a variety of levels of confinement, such as those that may be found within tissues *in vivo*, we find that MyoIIA is a key player in facilitating rapid motility and the ability to

Author Manuscript Author Manuscript Author Manuscript Author Manuscript

release from one surface contact and move to another. As in 2D environments, MyoIIA allows cells under confinement to maximize their speed. Importantly, the primary determinant of this optimum is an ideal degree of confinement coupled with MyoIIA function, and this optimum is less dependent upon integrin density than in 2D mesenchymal models. Using total internal reflection fluorescence (TIRF) imaging, we show that, under these optimal conditions, T cells migrate via a 'walking' mode. This MyoIIA-dependent motility mode permits T cells to make selective contacts with the substrate, minimizing their effective drag and allowing rapid movements between surfaces and in complex and dense environments.

RESULTS

T cells from MyoIIA conditional knockout mice

We previously showed that T lymphocytes alternate between 'walking' and 'sliding' modes of motility based in part on MyoIIA activity14 and we sought to determine how these mechanisms functioned in interstitial environments. MyoIIA (also called NMM-IIA) is the only class-II myosin expressed in murine T cells13 and germline knockout (KO) results in embryonic lethality17. To eliminate MyoIIA specifically from naïve T cells we employed a Cre recombinase-mediated conditional KO strategy targeting the MyoIIA heavy-chain gene (*Myh9*) (Supplemental Fig. 1). MyoIIA expression was deleted during the single-positive stage of thymocyte development by crossing MyoIIA floxed mice with a transgenic mouse line expressing Cre recombinase under control of a modified distal Lck promoter18 (Lck-Cre). As controls for our experiments, we used either MyoIIA$^{wt/wt}$-Lck-Cre^{+} mice or MyoIIA$^{flox/flox}$-Lck-Cre^{-} mice and obtained similar results with each. Single-positive CD4 and CD8 thymocytes appeared at normal percentages in the MyoIIA$^{flox/flox}$-Lck-Cre^{+} (hereafter referred to as MyoIIA cKO) (Fig. 1**a**, top). Mature T cells were present in the periphery, although CD8^{+} T cells in MyoIIA cKO mice were reduced compared to control mice (Fig. 1**a**). On average, CD8^{+} T cells in lymph nodes were 22.1% in control mice vs. 13.9% in MyoIIA cKO mice, and 13.9% vs. 7.0% in the blood. The lower numbers were likely due to reduced long-term survival of the MyoIIA-deficient CD8^{+} T cells in the periphery rather than a thymic exit defect given the normal thymic populations. Furthermore, when the percentage of MyoIIA cKO CD8^{+} T cells is ratioed to control mice in the lymph nodes (63% of control) vs. the blood (50% of control) this suggests a trend towards accumulation of CD8^{+} T cells in the lymph nodes of MyoIIA cKO mice.

The total pool of naïve CD8^{+} MyoIIA cKO T cells expressed one third of the MyoIIA protein detected in control cells (Fig. 1**b**). This was apparently the result of partial Cre expression in this population since, on average, ~85% of MyoIIA cKO CD8^{+} T cells had greatly reduced protein expression of MyoIIA but a sub-population of ~15% of CD8^{+} T cells had MyoIIA expression similar to control cells (Fig. 1**c**). To confirm the efficacy of our conditional KO approach and the penetrance of Cre expression in T cell populations, we crossed control and MyoIIA cKO mice to transgenic mice containing a knock-in of yellow fluorescence protein (YFP) in the Gt(Rosa)26Sor locus19 (Rosa-YFP mice). In these mice, YFP expression is dependent upon Cre expression as a result of an upstream stop codon cassette flanked by *loxP* sites. We determined that in control and MyoIIA cKO mice Cre

Author Manuscript Author Manuscript Author Manuscript Author Manuscript

expression was present in 80–95% of $CD8^+$ T cells but only in 50–60% of $CD4^+$ T cells (Fig. 1**d**). Immuno-blot analysis of sorted Rosa-YFP^+ control and MyoIIA cKO $CD8^+$ T cells routinely demonstrated a ~90% reduction of MyoIIA protein expression in Cre^+-$CD8^+$ T cells from MyoIIA cKO mice (Fig. 1**e**). This confirmed efficient MyoIIA depletion in Cre expressing $MyoIIA^{flox/flox}$ cells. It is possible that upon MyoIIA depletion other class-II isoforms could be upregulated in T cells. However, Myosin-IIB (*MyH10*) or Myosin-IIC (*MyH14*) protein expression was not detected in sorted Rosa-YFP^+ control and MyoIIA cKO $CD8^+$ T cells (Fig. 1**f**). Based on our results on Cre penetrance in $CD4^+$ versus $CD8^+$ T cell subsets we focused our work on the motility of $CD8^+$ T cells. To avoid subjecting naïve T cells to cell sorting, and given that on average 85% of $CD8^+$ T cells from MyoIIA cKO mice were highly depleted for MyoIIA, we used total $CD8^+$ T cells for our subsequent experiments.

MyoIIA regulates adhesion under flow

Analysis of differentially labeled transferred MyoIIA-deficient and control T cells did not show a gross alteration of their overall localization within lymph node T cell zones 2 hours after transfer. However, loss of MyoIIA resulted in a ~60% increase in the frequency of contact of MyoIIA cKO naïve T cells with high-endothelial venules (HEVs) at this time point (Fig. 2**a,b**). Rolling and firm-adhesion are critical steps for T cell extravasation, and a possible reason for the observed accumulation of MyoIIA cKO cells at HEVs could be increased adhesion, particularly under flow. Therefore, we measured the ability of MyoIIA-deficient T cells to adhere and remain attached to ICAM-1 coated surfaces in the presence of chemokine under physiological shear flow. Naïve MyoIIA cKO T cells had a 2-fold increase in adhesion to ICAM-1 under flow (Fig. 2**c**), confirming our findings of over-adhesion *in vivo*. However, when we next measured the ability of MyoIIA-deficient naïve T cells to transmigrate through endothelial cell monolayers plated on transwell membranes, MyoIIA cKO naïve T cells had a 2-fold inhibition of migration across endothelial cells (Fig. 2**d**). To rule out the possibility that the increased adhesion of MyoIIA-deficient T cells *in vitro* and *in vivo* was due to altered surface expression of chemokine or adhesion receptors we verified that control and MyoIIA-deficient T cells had similar expression of CCR7, L-selectin (CD62L) [http://www.signaling-gateway.org/molecule/query?afcsid=A001417] and the integrin LFA-1 (Fig. 2**e**).

MyoIIA controls interstitial T cell motility *in vivo*

To address how modulation of acto-myosin dynamics by MyoIIA affected T cell interstitial migration in the lymph nodes, we employed 2-photon microscopy analysis of adoptively transferred control and MyoIIA cKO $CD8^+$ T cells. MyoIIA cKO T cells had significantly shorter track lengths and reduced displacement from their origin (Fig. **3a–b** and Supplemental Movie 1). MyoIIA-deficient cells showed a 26% average reduction of their median speed and a decreased frequency of cells reaching peak instantaneous velocities (Fig. 3**c**). The median turning angle between time-points of MyoIIA cKO T cells was also increased from 47.5 to 54 degrees per turn (Fig. 3**d**). While these defects were numerically modest, they compounded over time and resulted in an average 45% reduction of the mean square displacement of MyoIIA-deficient T cells over a 10 min time period (Fig. 3**e**).

Author Manuscript Author Manuscript Author Manuscript Author Manuscript

Furthermore, the average motility coefficient, used as a measure of the volume a cell can survey over time20, was reduced by 49% (P=0.009) in MyoIIA cKO T cells from 27.7 to 14.2 μm/√min over a 10 min time period. MyoIIA cKO T cells also had an increased frequency of arrested cells (26.8% vs. 11.6%; P=0.0118), defined as cells that do not move more than 10μm from their origin during a ≥5 min interval.

The increased confinement of MyoIIA cKO T cells could be attributed to an inability to sense and follow a directional chemotactic cue. To assess this we measured both chemotactic (response to a directional gradient of chemokine) and chemokinetic (response to the presence of chemokine) migration of control vs. MyoIIA-deficient T cells across 5 μm pore 'transwells'. MyoIIA cKO T cells showed a 64% reduction in chemotaxis to CCL21 relative to control cells (Fig. 3**f**). However, chemokinesis was inhibited to the same extent, suggesting that the migration defects were not exclusively due to impaired chemotaxis of MyoIIA-deficient T cells.

MyoIIA regulates naïve T cell lymph node recirculation

The transmigration and interstitial motility defects of MyoIIA-deficient T cells prompted us to characterize the role of this myosin in trafficking and recirculation of naïve T cells. Following adoptive transfer we observed an accumulation of MyoIIA-deficient naïve T cells in lymph nodes compared to control cells (Fig. 4**a**). This accumulation increased over time between 2 and 42h post-transfer to a maximum of 1.9-fold (Fig. 4**b**). This could potentially be caused by increased entry and/or reduced egress from lymph nodes. Our data on *in vitro* trans-endothelial migration (TEM) of MyoIIA cKO T cells argued against the possibility of increased entry. To test whether impaired lymph node exit played a role in this accumulation, we transferred control and MyoIIA cKO T cells and allowed them to equilibrate for 24h and then blocked further T cell entry in the lymph nodes with blocking antibodies against CD62L. MyoIIA-deficient T cells showed a 3.3-fold increased retention in mice treated with CD62L antibodies compared to 1.8-fold in the absence of entry blockade (Fig. 4**c**). This indicated that MyoIIA plays a role in T cell exit rate from lymph nodes. Given the increased adhesion to ICAM-1 and on HEVs of MyoIIA cKO T cells, we also used LFA-1 and α_4 integrin blocking antibodies to rule out the possibility that MyoIIA cKO T cells could be entering lymph nodes even after CD62L blockade. A 3.2-fold increase of MyoIIA-deficient T cells relative to control cells under this blockade confirmed that accumulation of MyoIIA cKO cells was largely due to lymph node retention (Fig. 4**d**). MyoIIA-deficient T cells did not show a significant increase in accumulation at the surface of lymphatic sinuses (Fig. 4**e,f**), suggesting that reduced lymph node exit was likely due to increased interstitial confinement of MyoIIA-deficient T cells rather than to deficiencies in passage through the sinuses.

Optimal confinement and MyoIIA maximize motility

Given the 3D organization of the lymph node, and that directional chemotaxis of MyoIIA cKO T cells was not completely abrogated, we hypothesized that the MyoIIA-dependent migration defects could be caused by over-adherence to surrounding surfaces in confined environments. Therefore, we sought a method to dissect the role of cellular adhesion and contractility during migration in 3D environments as a contributor to the *in vivo* migration

Author Manuscript Author Manuscript Author Manuscript Author Manuscript

defects of MyoIIA cKO T cells. For this purpose, we employed micro-fabricated channels21 (microchannels) of varying size to provide a platform in which T cells can be variably confined in two dimensions while allowing motility in the third (Fig. 5**a**). We created these channels with a constant 'ceiling' height and with variable width to either confine the cells or allow them to meander to different degrees from side wall to side wall (Fig. 5**b** and Supplemental Movie 2). Microchannels can be assembled on glass coverslips, allowing imaging of the details of the adhesive contacts (using TIRF microscopy) on one surface during migration and extrapolation of the nature of these contacts to the other dimensions. We used activated T cells for the majority of these experiments as they had MyoIIA-dependent defects comparable to naïve T cells when analyzed both *in vivo* (Supplemental Fig. 2) and during transmigration *in vitro* (data not shown).

First we analyzed whether the degree of confinement affects T cell motility. For these experiments we used microchannels with a fixed ceiling height of 7μm, a dimension similar to the girth of an activated T cell. We also determined how different adhesiveness of the substrate may influence confined T cell migration by coating the microchannels with fibronectin, ICAM-1 or casein (which is not an integrin ligand and blocks integrin ligand binding to the substrate) (Fig. 5**c–e**). In all cases, we observed peak velocities at optimal confinement and reduced speeds when cells were too tightly or too loosely enclosed. In microchannels with widths that approximate their girth (7–9 μm), T cells migrated at peak average velocities that exceeded 20 μm/min in the presence of the integrin substrates fibronectin and ICAM-1 (Fig. 5**c,d**). T cell speed was reduced at smaller microchannel widths (4–5 μm), likely due to increased cell surface 'friction' along the channel walls. The other extreme of reduced confinement (12–20 μm microchannels) was also non-optimal, as we observed reduced speeds potentially due to sub-optimal availability of surfaces to 'push-off' and adhere-to, or to inefficiencies associated with protrusions in directions orthogonal to the direction of propagation.

Importantly, while T cells migrating in casein coated microchannels did not achieve the same average speeds detected in fibronectin and ICAM-1 coated microchannels, we still observed a similar confinement-dependent distribution of migration velocities in control cells (Fig. 5**e**). This suggested that confinement is a primary determinant of motility speed, and only to a lesser extent is the presence of integrin substrate necessary to achieve this optimum.

To characterize the role of MyoIIA in migration within microchannels we used the class-II myosin chemical inhibitor blebbistatin22, using imaging conditions that avoid photo-inactivation and toxicity of this drug (see **Methods**). Blebbistatin gave us the ability to acutely and completely inhibit the function of MyoIIA, complementing the MyoIIA cKO approach. Under these conditions, inhibition of MyoIIA resulted in an overall reduction of motility of activated T cells across all microchannel sizes with average speeds that did not significantly change relative to the confinement level (Fig. 5**c–e**). In particular, under conditions in which control cells achieve maximal motility (7–8 μm microchannels), MyoIIA-inhibited T cells did not significantly increase their average speed compared to microchannels with higher or lower confinement levels. This suggested that MyoIIA function is required not only for fast motility in general but specifically for T cells to 'adapt'

Author Manuscript Author Manuscript Author Manuscript Author Manuscript

their motility mode to the environment. Furthermore, since we observed similar motility rates when MyoIIA was blocked in the casein and integrin-substrate coated conditions, we conclude that MyoIIA function in optimizing motility is not strictly dependent on integrin binding to the substrate.

Further analysis of T cell motility within larger microchannels (greater than a cell width) coated with fibronectin provided additional evidence to support a complex interplay of surface contacts. In this setting, activated T cells constantly switched adherence ('weave') between opposing walls of the microchannel rather than crawling forward along one of the channel walls (Fig. 6**a**, **left,** and Supplemental Movie 3). Such 'weaving' could result from a T cell analogue of the 70 degree average bifurcation in the protrusions generated during motility in *Dictyostelium*23. MyoIIA-inhibited T cells became more adherent to the channel walls in-between 'weaves', resulting in a marked reduction of the 'weaving' frequency (Fig. 6**a**, **right,** and Supplemental Movie 4). Blebbistatin-treated T cells doubled the time elapsed from initial adhesion to one side wall of the channel to contacting the other ('weaving' cycle) (Fig. 6**b**, **left panel**). This was not a function of the slower velocity of MyoIIA cells in the presence of blebbistatin as shown by the fact that the adhesion time to a channel wall of MyoIIA-inhibited T cells was also doubled (Fig. 6**b**, **right panel**). In sum, these experiments indicated that MyoIIA functions to limit adhesion to the substrate for confinement-optimized motility.

To specifically analyze the nature of the coupling of cells to surfaces under 3D confinement, we used TIRF microscopy of T cells in microchannels to visualize the adhesive contacts on the surface nearest the objective. We previously observed that loss of MyoIIA resulted in a shift in the crawling mode of $CD4^+$ T cell clones during 2D migration, which was associated with increased adherence14. TIRF imaging of activated control T cells in microchannels indicated that these cells migrated predominantly using amoeboid crawling with multiple small independent surface contact points ('walking') (Fig. 6**c,d**, **and** Supplemental Movie 5). Thus, although cells appear elongated, they are effectively choosing only select points of the membrane for surface contact, thereby potentially limiting frictional drag while permitting dynamic scanning of new areas. Blebbistatin-induced loss of MyoIIA activity resulted in a change of motility mode, with T cells predominantly crawling using one large adhesion area ('sliding') and with prolonged contacts on a given microchannel wall (Fig. 6**c,d**, **and** Supplemental Movie 6). While still capable of forward crawling, this mode results in an increased 'drag surface' involving a greater portion of the cell cortex and likely slowing down the cell.

Finally, although technically challenging, due to their reduced motility and entry into microchannels, we also analyzed naïve T cell migration in microchannels (using a 3μm ceiling height due to their smaller size). Generally, compared to activated T cells, naïve T cells were less motile, particularly under reduced confinement (>10μm channels) (Supplemental Fig. 3); this also confirmed that larger channels do not support optimal motility rates. Nonetheless, comparing control and MyoIIA cKO naïve T cell migration in 4 and 8μm wide microchannels supported a role for MyoIIA as a determinant in optimizing T cell motility in confinement (Supplemental Fig. 3).

Author Manuscript Author Manuscript Author Manuscript Author Manuscript

Over-adhesion of MyoIIA-deficient T cells

TIRF microscopy showed a significant increase in the adhesion area of blebbistatin-treated activated $CD8^+$ T cells relative to control cells when plated on casein or ICAM-1 coated surfaces (Fig. 7**a,b**). This was also true for MyoIIA cKO naïve $CD8^+$ T cells compared to control cells plated on ICAM-1 (Fig. 7**c**). The adhesion area of naïve T cells plated on casein coated surfaces was too small to be consistently detected using our TIRF imaging method. Furthermore, similar to our previous observations13, inhibition of MyoIIA also resulted in altered cell morphology with increased rounding of activated T cells as shown by measuring their 'shape factor' (indicating how circular a cell is) and 'ellipticity' (length/breadth of the cell) (Supplemental Fig. 4). Overall, these data are consistent with a role for MyoIIA in modulating T cell surface contacts, both in the presence and absence of integrin ligands.

In vivo within the lymph node paracortex, T cells are believed to follow tracks defined by a dense network of fibroblastic reticular cells24 (FRCs), and it has been shown that FRCs can provide chemokines to support adhesion and migration of T cells25,26. Therefore, we tested whether over-adhesion of T cells in the absence of MyoIIA function would result in increased contact with FRCs and cause the slower and more meandering motility of MyoIIA cKO T cells *in vivo*. To determine the extent of adhesion of T cells to FRCs *in vivo* we generated bone marrow chimeric mice by reconstituting irradiated actin promoter-CFP mice with bone marrow cells from wild type mice (as described in24). Imaging of labeled control and MyoIIA cKO cells transferred into the chimeric mice did not reveal a significant difference in the percentage of MyoIIA cKO naïve T cells potentially interacting with FRCs within lymph nodes compared to control cells (Fig. 7**d**).

We therefore considered other cells present in lymph nodes as candidates for adhesion and frictional drag. We quantified the adhesion of T cells to other lymph node dwelling cells such as lymphatic endothelial cells (LECs), dendritic cells (DCs), and other T cells. Our *in vitro* coupling data confirmed that MyoIIA-deficient naïve T cells do not have increased interaction with FRCs and showed that the percentage of attachment to LECs and DCs was also similar to control T cells (Fig. 7**e**). However, MyoIIA cKO T cells had a ~60% increase in the attachment to other T cells compared to control cells (Fig. 7**e**, right). In the T cell zones of lymph nodes T cells are likely to be constantly in proximity with other surrounding lymphocytes and these prolonged interactions would be predicted to cause excessive drag resulting in reduced motility and increased meandering *in vivo*.

DISCUSSION

Lymphocyte migration *in vivo* relies on coordinated regulation of actin polymerization and branching, as suggested by work on T cells deficient in upstream regulators of Arp2/3 such as WASP27, Dock228, and Coronin-1A29,30. On the other hand, the role of class-II myosin during interstitial T cell migration was previously unknown. Our work is the first indication of a requirement for MyoIIA function in lymphocyte migration and trafficking *in vivo*. Importantly, it provides novel insight into the extent and dynamics of surface contacts as important factors regulating 3D lymphocyte migration.

Author Manuscript Author Manuscript Author Manuscript Author Manuscript

Microfabricated channels enabled us to recapitulate some aspects of environmental confinement that lymphocytes may encounter *in vivo* and permitted us to demonstrate the existence of a confinement optimum for amoeboid motility. The presence of integrin ligands had only a limited effect on this optimization, in contrast to what is predicted from the haptokinetic model and in agreement with recent studies of leukocyte migration in vivo7,9. Indeed, faced with low adhesive substrates, amoeboid cells can adapt by increasing actin polymerization rates during protrusion to compensate for reduced force-coupling31. This is also consistent with the idea of 'chimneying' described in cells crawling between adjacent coverslips32.

Under ideal confinement, we observed migration speeds greater than 20μm/min; these are higher than average speeds but equivalent to the fastest instantaneous speeds reported for motility in lymph nodes. This could be due to the fact that individual microchannels provide a consistent and in some cases optimized (i.e. ~8μm channels) environment for T cell migration. In contrast, within lymph nodes, lymphocytes likely encounter varying microenvironments with different characteristics which may modulate motility speeds and limit peak velocities.

Furthermore, in the absence of MyoIIA function T cells can't achieve optimal motility within microchannels, likely due to hyper-adhesion and spreading which cause increased friction and drag. In this light, MyoIIA regulation of cortical tension and adhesion can modulate the ability of lymphocytes to adapt their morphology to optimize their interaction with the environment during motility.

We propose that the motility optimum is reached at confinement levels where three things coincide. First, the ability to contact and exert force on multiple adjacent surfaces is maximized, optimizing frictional coupling without the need for highly specific protein-protein interactions. Second, inefficiencies from actin-based protrusion along incorrect axes are minimized. Third, the cell can restrict the extent of cortical contact with the substrate, minimizing excessive drag. Under extreme confinement, the size and rigidity of the nucleus may limit how thin the cell can become, forcing the cortex to drag along even when not in use for force-coupling. It has previously been proposed that MyoIIA might overcome such nuclear-induced drag when dendritic cells migrate through dense collagen matrices7. That report, however, speculated that MyoIIA functioned as a 'squeezing' force which may be a separate function for this motor.

Morphologically, the 'walking' mode facilitated by MyoIIA utilizes multiple contacts that may be somewhat similar to the 'eupodia' described in *Dictyostelium*33. We previously showed by molecular imaging that clusters of MyoIIA moved inward towards the center of these contacts and that this movement was coincident with the extinguishing of the contact and release from the substrate14. Our data is in agreement with work showing that 2D motility in the amoeba *Dictyostelium* relies on myosin-II contractility to provide cortical tension and de-adhesion from the substrate34. Further evidence for MyoIIA in disassembling actin and thereby potentially functioning to extinguish cortical adhesive contacts with the substrate has recently been reported35. A 'millipede' motility mode during migration along the inner face of HEVs36 may also be a variant of this 'walking' mode.

Author Manuscript Author Manuscript Author Manuscript Author Manuscript

A general theme emerging from our work is a role for MyoIIA in controlling adhesion independently of substrate composition. Thus, T cells lacking MyoIIA over-adhere to HEVs, other T cells, and artificial substrates, whether coated with integrin ligands or blocked from integrin binding. This is partly consistent with reports suggesting that MyoIIA plays a role in uropodal detachment from highly adhesive integrin ligand-coated 2D surfaces15,16. This has been proposed to involve MyoIIA linkage to LFA-1 to mediate de-attachment, without affecting LFA-1 affinity regulation15. While not excluding such a possibility, we prefer the interpretation that MyoIIA's role in adhesion may be indirect, and not strictly linked to integrin adhesion. The specific effects that were confined to the uropod in the previous studies could be due to the specific adhesive properties of the surfaces, cells, or drugs used in these different experimental systems.

In sum our data suggests that the increased turning and reduced velocity of MyoIIA cKO T cells *in vivo* may be determined by a diminished capacity to limit contacts with their environment. We did not find evidence that the FRC network was a substrate for this increased adhesion *in vivo*. On the other hand, our results indicated that the over-adhesive properties of MyoIIA-deficient T cells can cause an abnormal level of attachment to other T lymphocytes. In the lymph node, even brief spreading of the cell cortex of one T cell onto the cortex of another, particularly when moving with opposite trajectories, would oppose efficient forward movement.

While it has been reported that loss of MyoIIA can affect neutrophil polarity37, and alter T cell morphology13, our data suggests that loss of polarity is not the primary defect of MyoIIA-depleted T cells. In particular, within microchannels we did not observe excessive directional changes of MyoIIA-inhibited cells, and the reduced response to a chemotactic gradient is likely secondary to their over-adhesion.

Overall, our findings suggest that by limiting surface adhesion and providing contractile force, MyoIIA optimizes lymphocyte crawling efficiency within the multiple environments that T cells must pass through during their trafficking. In contrast to an integrin-only mediated switch in motility rate as predicted by haptokinetic models, we propose a switch in motility rate affected by the density (degree of confinement) of the tissue and by modulation of MyoIIA function. Such a motility switch for T cells might also occur during early activation which leads to phosphorylation of the myosin heavy chain in response to calcium signaling13. This can result in the reorganization of myosin filaments38, leading to the regulation of the ability of MyoIIA to crosslink and contract the actin network. Modulation of MyoIIA activity can therefore be considered as an important regulator of T cell trafficking and potentially surveillance by modulating cell stopping.

METHODS

Targeting vector and generation of MyoIIA heavy-chain (*Myh9*) floxed allele

An XbaI/NsiI genomic fragment containing exon 3 of the *Myh9* locus plus flanking introns cloned into pBluescript was used for construction of the targeting vector. An NdeI/SphI fragment was cut out of this clone, blunt-ended and subcloned into the blunt-ended HindIII site between the 5' loxP site and the neomycin resistance cassette of the vector pBS479 (a

Author Manuscript Author Manuscript Author Manuscript Author Manuscript

kind gift of B. Sauer, Stowers Institute for Medical Research, Kansas City, MO). A NotI/NotI fragment containing the genomic sequence, loxP sites and the neomycin cassette was then cut out of pBS479, blunt-ended and re-inserted into the blunt-ended NdeI/SphI cut targeting vector. In making this construct, a 208bp SphI fragment, at a distance of 949bp 3' of the end of exon 3, was deleted. A diphtheria toxin (DTA) cassette was also present in the SalI site of pBluescript, at the 3' end of the genomic sequence. The presence of the genomic locus, neomycin resistance cassette, and DTA was determined by restriction enzyme mapping and confirmed by sequencing of the construct. Embryonic stem (ES) cells were targeted by homologous recombination and mice were generated using conventional means. Genomic DNA from ES cell colonies and F1 generation mice was screened by PstI digestion and Southern blotting with the probe indicated in Supplemental Fig. 1 (MyoIIA^{wt} allele, 6.2kb; MyoIIA^{flox} allele, 3.8kb).

Mice

Mice containing the MyoIIA heavy-chain (*Myh9*) floxed allele were crossed with mice expressing Cre recombinase under the control of a modified *Lck* distal promoter18 (Lck-Cre mice), developed by Nigel Killeen (UCSF). Littermate or age-matched MyoIIA$^{wt/wt}$-Lck-Cre^{+} or MyoIIA$^{flox/flox}$-Lck-Cre^{-} mice were used as controls. The experimental mice were on a mixed C57BL/6J-129 background. C57BL/6J × 129S1 F1 mice (cat. #101043) were used as recipient mice for adoptive transfers and were purchased from Jackson Laboratories. OT-I TCR transgenic mice and Actin-promoter CFP mice were also purchased from Jackson Laboratories and bred in our facilities in accordance with the guidelines of the Laboratory Animal Resource Center of the University of California at San Francisco. All experiments involving mice were approved by the Institutional Animal Care and Use Committee of the University of California.

Generation of actin promoter-CFP chimeric mice

The chimeric mice were generated following the protocol previously established by the Germain lab24. Briefly, we γ-irradiated (2× 600 rads) actin promoter-CFP mice and reconstituted them with 5–10×10^{6} bone marrow cells from wild type mice. The chimeric mice were allowed to reconstitute for a minimum of 8 weeks before use as recipient mice in 2-photon experiments to visualize cells of non-hematopoietic origin in the lymph node.

Cells

Naïve T cells were purified from lymph nodes and spleens using the StemSep CD8 T cell negative selection kit (Stem Cell Technologies). Activated primary CD8^{+} T cells were obtained by stimulation of lymphocytes derived from OT-I TCR transgenic mice on CD3 and CD28 coated plates; cells were used 4 or 5 days after stimulation. Activated MyoIIA-depleted T cells were obtained by transduction of T cells from MyoIIA$^{flox/flox}$ mice with retrovirus0065s encoding either Cre-GFP (to eliminate MyoIIA expression) or GFP only (as a control) 48h after initial activation. 72h post-transduction GFP^{+} T cells were sorted and used for experiments; depletion of MyoIIA in the Cre-transduced T cells was routinely verified by immuno-blotting or FACS analysis. T cells were cultured using RPMI 1640 (Invitrogen) with the addition of 10% FCS and L-glutamine, penicillin, streptomycin and β-

Author Manuscript Author Manuscript Author Manuscript Author Manuscript

mercaptoethanol. Activated T cells were cultured in complete RPMI with the addition of 10 U/ml of Interlukin-2.

T cell labeling and adoptive transfer

Purified control and MyoIIA cKO T cells were labeled with either CFSE or CMTMR for 25 min, washed 3 times, and then used in the various assays. All experiments were repeated switching dye-labeling of control and MyoIIA cKO T cells with equivalent results. $3–5\times10^6$ T cells were adoptively transferred by intravenous tail vein injection into C57BL/6J × 129S1 F1 recipients to avoid potential rejection of transferred cells due to their mixed background.

Antibodies and reagents

Rabbit polyclonal anti-class II Myosin (BTI) was used for immunofluorescence and immuno-blotting. PNAd-1 (Meca-79), CD62L (Mel-13) antibodies were from BD Biosciences. Integrin Alpha-4 (PS/2) and LFA-1 (M17/4) antibodies were from Bio-X-cell. Lyve-1 goat polyclonal antibodies were from R&D Systems. CD4 (GK1.5) and CD8 (YTS169.4) monoclonal antibodies conjugated to FITC, PE, or PerCP were purchased from BD Biosciences. Anti-CCR7-biotin (4B12) was purchased from BioLegend. Unconjugated CD16/CD32 (24G.2), and CD4 (GK1.5), CD8 (YTS169.4), CD62L (Mel-13), LFA-1 (M17/4) monoclonal antibodies conjugated to Alexa-647 (Invitrogen) were made by the UCSF Hybridoma Core Facility. Fluorophore-conjugated secondary antibodies were purchased from Jackson Immunoresearch Laboratories. Mouse monoclonal anti-tubulin, aprotinin, leupeptin, phenylmethylsulfonyl fluoride (PMSF), sodium fluoride, iodoacetamide and sodium orthovanadate were purchased from Sigma. Horseradish peroxidase–conjugated protein A and detergent-compatible protein assay kit were purchased from Bio-Rad. CFSE and CMTMR were purchased from Invitrogen. Blebbistatin (racemic mix) was from Calbiochem and was used at 100 μM of the racemate. Casein (Sigma) and ICAM-1-Fc (R&D Systems) were used to coat glass chamberslides and microchannels (Nalge Nunc International) at a concentration of 40 nM for 1 h at 37°C.

Flow cytometry

Single cell suspensions from dissociated thymii, lymph nodes and spleen were blocked with anti-CD16/CD32 for 10 min at 4°C and then stained for 25 min at 4°C. Samples were then washed and acquired using a FACS Calibur (BD Biosciences) and analyzed using Cell Quest (BD Biosciences) or FlowJo (Tree Star).

Immuno-blotting

Immuno-blotting was routinely performed as previously described13 to quantify the level of MyoIIA knockdown in T cells. Tubulin immuno-blotting was performed as a control to normalize MyoIIA knockdown densitometry.

Two-photon microscopy

We used a custom resonant scanning two-photon instrument with an array of four R5929 photomultiplier tubes (Hamamatsu) operating at video rate39. For image acquisition a custom four-dimensional acquisition module in the VideoSavant digital video recording

Author Manuscript Author Manuscript Author Manuscript Author Manuscript

software (IO Industries) was used39. To image CFSE and CMTMR labeled lymphocytes, samples were excited with a 5-W MaiTai TiSaphire laser (SpectraPhysics) tuned to 810 nm wavelength and fitted with a FemtoControl pulse compressor (APE). Emission wavelengths of 380–420 nm (for collagen derived second-harmonic emission), 500–550nm (for CFSE - green), and 567–640 nm (for CMTMR - red) were acquired. For time-lapse image acquisition, each xy plane spanned 288 μm × 240 μm at a resolution of 0.60 μm/pixel. Images of up to 40 xy planes with 3 μm z-spacing were acquired every 20 seconds for 30 min.

Purified control and MyoIIA cKO naïve $CD8^+$ T cells (3–5 × 10^6 each), labeled with either 2 μM CFSE or 20 μM CMTMR, were mixed at a 1:1 ratio and adoptively transferred by intravenous tail vein injection into C57BL/6J × 129S1 F1 recipients or in actin promoter-CFP chimeric mice (obtained as described above). 18 or 42 hours following T cell transfer, recipient mice were sacrificed and popliteal, inguinal and axillary lymph nodes were surgically removed and immobilized on coverslips with the medullary side adhered to the coverslip. Lymph nodes were maintained between 35.5 −37°C in a flow chamber perfused with RPMI medium without phenol red (Gibco) saturated with a 95% O_2/5% CO_2 gas mixture.

Imaris software (Bitplane AG) was used to analyze the 3D data and to track cells. Imaris and Matlab software (Mathworks) were then used to obtain T cell speed, turning angle and mean square displacement. Instantaneous velocities and turning angle distributions were calculated between two (velocity) and three (turning angle) consecutive timepoints for each time point of each cell in a stage position. The average median velocity and turning angles were calculated on a per cell basis and the average of all cell values was then calculated. The mean square displacement over a 10 min time period was calculated for each cell in a stage position and the average for each stage position was then determined; finally, the average of all stage positions from three independent experiments was calculated. The motility coefficient for each cell population in a stage position was then determined by calculating the slope of the mean square displacement curve and applying the formula: motility coefficient = $x^2/6t$, with x being the slope of the MSD curve.

Transwell migration assay

Purified naïve $CD8^+$ T cells from control and MyoIIA cKO mice were labeled with either 1 μM CFSE or 10 μM CMTMR, mixed at a 1:1 ratio and used for transwell migration assays. 10^6 labeled T cells resuspended in RPMI supplemented with 1% fatty acid-free BSA (Calbiochem) and 10 mM HEPES were added to the top chambers of transwell plates (Corning) and allowed to migrate for 1h at 37° C in the presence or absence of chemokine. Migrated T cells were then collected from the bottom wells and quantified for a fixed period of time (2–3 min) on a FACS Calibur (BD Biosciences). Known amount of cells, acquired for the same amount of time, were used as standards to determine the number of migrated cells.

Author Manuscript Author Manuscript Author Manuscript Author Manuscript

Lymph node staining

2 and 48h after adoptive transfer of control and MyoIIA cKO naïve T cells, labeled with either 1 μM CFSE or 10 μM CMTMR, the popliteal lymph nodes of recipient mice were harvested and snap frozen in OTC compound (Tissue-Tek). 10 μm-thick sections of the lymph nodes were fixed with 1% para-formaldehyde (PFA), blocked and stained. PNAd-1 antibodies were used to visualize high endothelial venules (HEVs), while Lyve-1 antibodies were used to highlight lymphatic sinuses. Images of whole lymph node sections were acquired on a confocal microscope using the scan-slide function of Metamorph (Universal Imaging). The data was then analyzed using Imaris software to identify T cells based on their CFSE or CMTMR fluorescence and then creating a surface mask of the stained HEVs or lymphatic sinuses. The percentage of T cells in contact with HEV surfaces or lymphatic sinuses was then quantified using the 'spot-to-surface distance' function of Imaris. Multiple lymph node sections were analyzed with an average of 50 cells for each group per lymph node section. An average of 4 lymph node sections per experiment was analyzed.

T cell lymph node homing and egress

Control and MyoIIA cKO T cells were labeled with either 1 μM CFSE or 10 μM CMTMR, mixed at a 1:1 ratio, and $2–4\times10^6$ T cells were injected intravenously into recipient mice. At 2, 18 or 42h after adoptive transfer, lymph nodes, blood and spleen were harvested from the recipient mice. After lymph node and spleen dissociation, the percentage of transferred control and MyoIIA cKO T cells was quantified by FACS and the ratio of cKO vs. control T cells in the blood, inguinal lymph nodes and spleen of recipient mice was determined. The ratios for the lymph node and spleen were normalized to the ratio in the blood to correct for potential differences in the input or survival of control vs. MyoIIA cKO cells.

To determine the egress rate and lymph node retention of control vs. MyoIIA cKO T cells, transferred T cells were allowed to equilibrate for 24h in recipient mice and then the mice were treated with PBS or entry-blocking antibodies. CD62L antibodies or a combination of LFA-1 and integrin α_4 antibodies were used with similar results. 18h after the blocking antibody treatment, the ratio of MyoIIA cKO vs. control T cells retained in the inguinal lymph nodes of recipient mice was determined as described above.

Adhesion to ICAM under flow

Control and MyoIIA cKO naïve $CD8^+$ T cells were labeled with either 1 μM CFSE or 10 μM CMTMR, mixed at a 1:1 ratio and injected into flow chambers (IBIDI) at 0.25 dyne/cm^2 shear flow for 2 min and then subjected to 10 min of physiological shear flow (2 dyne/cm^2). Brightfield and fluorescent images were then acquired and the number of adherent cells at the end time point was quantified with Metamorph software.

Microchannel fabrication and imaging

The microchannel fluidic devices were fabricated using a soft lithography technique with polydimethylsiloxane (PDMS) (Dow Corning Sylgard Elastomer 184 Kit) as described21. Briefly, PDMS was poured onto the stamp and left to cure overnight under vacuum; once solidified, the PDMS with the embedded microchannels was then cut out of the mold and an entry port was cut adjacent to the channel structures. The PDMS and a glass-bottom imaging

Author Manuscript Author Manuscript Author Manuscript Author Manuscript

dish (Fluoro Dish, World Precision) were then activated in a plasma cleaner (Harrick Plasma) for 30 sec and bonded to each other. After 1 hour incubation at 55° C, the microchannel imaging chambers were then put back in the plasma cleaner and left under vacuum for 5 min after which the plasma source was activated for 15 sec. Immediately after this step, 10 μl of a fibronectin solution (50 μg/ml), ICAM-1 (5μg/ml) or Casein (20μg/ml) solution was injected into the entry area of the microchannels to coat them. After 1h incubation at 37°C, the excess coating proteins were washed-out with PBS and imaging media was added. $1–3\times10^5$ T cells (resuspended in 10 μl) were then added to the entry port and the cells were allowed to spontaneously enter the channels at 37°C for 2–4h for activated T cells and overnight for naïve T cells. T cells crawling in the microchannels were then imaged using a phase contrast objective for 1–6h at 30 sec or 90 sec intervals. T cells remained alive and motile for the entire period of the recording. Metamorph (Molecular Devices) software was used to calculate cell speed, adhesion time and 'weave' cycle. Typically a minimum of 10 cells per microchannel width per treatment condition were analyzed.

TIRF microscopy

TIRF imaging was performed on a modified Axiovert 200M microscope fitted with a Zeiss TIRF slider and a 100X/1.45 NA oil immersion objective. TIRF images were acquired with a liquid-cooled intensified CCD camera (model XR/Mega-10Z) from Stanford Photonics. The TIRF microscope was equipped with 491 nm (50mW) and 561 nm (25 mW) solid-state lasers (Cobolt) and excitation wavelength was selected through an AOTF (Neos). Emission wavelengths were selected through the combination of a multiple-edge dichroic and multiple-pass emission filter. The control and imaging software was InVivo (QED Imaging/ Media Cybernetics). The microscope was configured with a heated stage to maintain sample temperature at 37°C.

For TIRF imaging of surface adhesion zones, activated T cells were labeled with 4 μM CMTMR. 5×10^4 T cells were plated overnight in glass chamberslides or, alternatively, 10^6 T cells were injected into variable size microchannels. For timelapse experiments, brightfield and TIRF fluorescence images were acquired every 5 sec for 5 min. To prevent photo-inactivation, cross-linking and toxicity of blebbistatin, which may occur when illuminated with <500 nm light40, TIRF imaging of blebbistatin treated cells was performed using CMTMR labeling and illuminating the cells with a 561 nm laser.

Contact area measurements were performed using Metamorph software, CMTMR fluorescence in the TIRF channel was thresholded, and the area of the fluorescent region was then calculated using the "region statistics" function of Metamorph. Determination of the crawling mode was performed as described14. Briefly, if the CMTMR TIRF fluorescence during the timelapse showed only one main adhesion area the cell was scored as "sliding"; if multiple distinct adhesion zones were present the cell was scored as "walking." A cell with multiple adhesion zones was scored as "mixed" if it presented a single adhesion zone consecutively for more than half of the duration of a timelapse. The 'shape factor' which indicates how closely a cell resembles a circle was calculated as: $(4 \times \pi \times \text{Area})/\text{Perimeter}^2$; with values close to 0 indicating an elongated cell and 1 representing a

Author Manuscript Author Manuscript Author Manuscript Author Manuscript

perfect circle. T cell 'ellipticity' was calculated as: cell length (span of the longest cord through the cell) / cell breadth (width of the cell perpendicular to the longest cord). These morphology parameters were calculated with Metamorph using the brightfield images acquired during TIRF imaging.

Stromal cell lines

Primary cell lines of lymphoid stroma were obtained by complete collagenase A and D digestion of C57BL/6J lymph nodes following a previously described protocol26. After complete digestion, the final cell pellet was sorted for FRCs ($CD45^-$,$CD35^-$, $CD31^-$, $gp38^+$) or LECs ($CD45^-$,$CD35^-$, $CD31^+$, $gp38^+$).

T cell coupling assay

Control and MyoIIA cKO naïve $CD8^+$ T cells were labeled with 1 μM CFSE and coupled to CMTMR (10 μM) labeled FRCs, LECs, DCs or wild-type T cells. For coupling, cells were briefly spun together for 1 min at 200g and incubated for 10 min at 37° C, gently resuspended and then fixed with 1% PFA. Cells were then washed and the percentage of conjugate formation was quantified by FACS.

Statistical analysis

Prism software (GraphPad) was used to graph the data and calculate statistical significance. The statistical significance of data was determined by performing either Student's t-test for single comparisons, or analysis of variance (ANOVA) for multiple comparisons, followed by post hoc Tukey tests on continuous variable data which was normally distributed and had equal variance. Alternatively, Kruskal-Wallis or Mann-Whitney tests were used for non-normally distributed data to determine statistical significance, followed by Dunn post-tests to determine p values for multiple comparisons. To determine the significance of nominal variable data the Chi-square test was used.

Supplementary Material

Refer to Web version on PubMed Central for supplementary material.

ACKNOWLEDGEMENTS

We thank P. Beemiller for help with 2-photon data analysis using Imaris and Matlab software. We thank S. Peck for assistance in maintenance of microscopes and S. Jiang for expert technical assistance with cell sorting. We thank O. Khan and M. Werner for help with mouse typing and M. Heuze (Institute Curie, Paris, France) for assistance in setting up the microchannel system. We thank B. Sauer (Stowers Institute for Medical Research, Kansas City, MO) for the kind gift of the pBS479 vector.

REFERENCES

1. Dustin ML. Stop and go traffic to tune T cell responses. Immunity. 2004; 21:305–314. [PubMed: 15357942]
2. von Andrian UH, Mempel TR. Homing and cellular traffic in lymph nodes. Nat Rev Immunol. 2003; 3:867–878. [PubMed: 14668803]

Author Manuscript Author Manuscript Author Manuscript Author Manuscript

3. Cahalan MD, Parker I. Choreography of cell motility and interaction dynamics imaged by two-photon microscopy in lymphoid organs. Annu Rev Immunol. 2008; 26:585–626. [PubMed: 18173372]
4. Bajenoff M, et al. Highways, byways and breadcrumbs: directing lymphocyte traffic in the lymph node. Trends Immunol. 2007; 28:346–352. [PubMed: 17625969]
5. DiMilla PA, Barbee K, Lauffenburger DA. Mathematical model for the effects of adhesion and mechanics on cell migration speed. Biophys J. 1991; 60:15–37. [PubMed: 1883934]
6. Palecek SP, Loftus JC, Ginsberg MH, Lauffenburger DA, Horwitz AF. Integrin-ligand binding properties govern cell migration speed through cell-substratum adhesiveness. Nature. 1997; 385:537–540. [PubMed: 9020360]
7. Lammermann T, et al. Rapid leukocyte migration by integrin-independent flowing and squeezing. Nature. 2008; 453:51–55. [PubMed: 18451854]
8. Woolf E, et al. Lymph node chemokines promote sustained T lymphocyte motility without triggering stable integrin adhesiveness in the absence of shear forces. Nat Immunol. 2007; 8:1076–1085. [PubMed: 17721537]
9. Friedl P, Entschladen F, Conrad C, Niggemann B, Zanker KS. CD4+ T lymphocytes migrating in three-dimensional collagen lattices lack focal adhesions and utilize beta1 integrin-independent strategies for polarization, interaction with collagen fibers and locomotion. Eur J Immunol. 1998; 28:2331–2343. [PubMed: 9710211]
10. Vicente-Manzanares M, Ma X, Adelstein RS, Horwitz AR. Non-muscle myosin II takes centre stage in cell adhesion and migration. Nat Rev Mol Cell Biol. 2009; 10:778–790. [PubMed: 19851336]
11. Lammermann T, Sixt M. Mechanical modes of 'amoeboid' cell migration. Curr Opin Cell Biol. 2009; 21:636–644. [PubMed: 19523798]
12. Pollard TD, Borisy GG. Cellular motility driven by assembly and disassembly of actin filaments. Cell. 2003; 112:453–465. [PubMed: 12600310]
13. Jacobelli J, Chmura SA, Buxton DB, Davis MM, Krummel MF. A single class II myosin modulates T cell motility and stopping, but not synapse formation. Nat Immunol. 2004; 5:531–538. [PubMed: 15064761]
14. Jacobelli J, Bennett FC, Pandurangi P, Tooley AJ, Krummel MF. Myosin-IIA and ICAM-1 regulate the interchange between two distinct modes of T cell migration. J Immunol. 2009; 182:2041–2050. [PubMed: 19201857]
15. Morin NA, et al. Nonmuscle myosin heavy chain IIA mediates integrin LFA-1 de-adhesion during T lymphocyte migration. J Exp Med. 2008; 205:195–205. [PubMed: 18195072]
16. Smith A, Bracke M, Leitinger B, Porter JC, Hogg N. LFA-1-induced T cell migration on ICAM-1 involves regulation of MLCK-mediated attachment and ROCK-dependent detachment. J Cell Sci. 2003; 116:3123–3133. [PubMed: 12799414]
17. Conti MA, Even-Ram S, Liu C, Yamada KM, Adelstein RS. Defects in cell adhesion and the visceral endoderm following ablation of nonmuscle myosin heavy chain II-A in mice. J Biol Chem. 2004; 279:41263–41266. [PubMed: 15292239]
18. Zhang DJ, et al. Selective expression of the Cre recombinase in late-stage thymocytes using the distal promoter of the Lck gene. J Immunol. 2005; 174:6725–6731. [PubMed: 15905512]
19. Srinivas S. Cre reporter strains produced by targeted insertion of EYFP and ECFP into the ROSA26 locus. BMC Dev Biol. 2001; 1(4):1–8. [PubMed: 11178105]
20. Sumen C, Mempel TR, Mazo IB, von Andrian UH. Intravital microscopy: visualizing immunity in context. Immunity. 2004; 21:315–329. [PubMed: 15357943]
21. Faure-Andre G, et al. Regulation of dendritic cell migration by CD74, the MHC class II-associated invariant chain. Science. 2008; 322:1705–1710. [PubMed: 19074353]
22. Straight AF, et al. Dissecting temporal and spatial control of cytokinesis with a myosin II Inhibitor. Science. 2003; 299:1743–1747. [PubMed: 12637748]
23. Andrew N, Insall RH. Chemotaxis in shallow gradients is mediated independently of PtdIns 3-kinase by biased choices between random protrusions. Nat Cell Biol. 2007; 9:193–200. [PubMed: 17220879]

Author Manuscript Author Manuscript Author Manuscript Author Manuscript

24. Bajenoff M, et al. Stromal cell networks regulate lymphocyte entry, migration, and territoriality in lymph nodes. Immunity. 2006; 25:989–1001. [PubMed: 17112751]
25. Hara T, et al. A transmembrane chemokine, CXC chemokine ligand 16, expressed by lymph node fibroblastic reticular cells has the potential to regulate T cell migration and adhesion. Int Immunol. 2006; 18:301–311. [PubMed: 16410312]
26. Katakai T, Hara T, Sugai M, Gonda H, Shimizu A. Lymph node fibroblastic reticular cells construct the stromal reticulum via contact with lymphocytes. J Exp Med. 2004; 200:783–795. [PubMed: 15381731]
27. Snapper SB, et al. WASP deficiency leads to global defects of directed leukocyte migration in vitro and in vivo. J Leukoc Biol. 2005; 77:993–998. [PubMed: 15774550]
28. Nombela-Arrieta C, et al. A central role for DOCK2 during interstitial lymphocyte motility and sphingosine-1-phosphate-mediated egress. J Exp Med. 2007; 204:497–510. [PubMed: 17325199]
29. Shiow LR, et al. The actin regulator coronin 1A is mutant in a thymic egress-deficient mouse strain and in a patient with severe combined immunodeficiency. Nat Immunol. 2008; 9:1307–1315. [PubMed: 18836449]
30. Foger N, Rangell L, Danilenko DM, Chan AC. Requirement for coronin 1 in T lymphocyte trafficking and cellular homeostasis. Science. 2006; 313:839–842. [PubMed: 16902139]
31. Renkawitz J, et al. Adaptive force transmission in amoeboid cell migration. Nat Cell Biol. 2009; 11:1438–1443. [PubMed: 19915557]
32. Malawista SE, de Boisfleury Chevance A. Random locomotion and chemotaxis of human blood polymorphonuclear leukocytes (PMN) in the presence of EDTA: PMN in close quarters require neither leukocyte integrins nor external divalent cations. Proc Natl Acad Sci USA. 1997; 94:11577–11582. [PubMed: 9326652]
33. Fukui Y, Inoue S. Amoeboid movement anchored by eupodia, new actin-rich knobby feet in Dictyostelium. Cell Motil Cytoskeleton. 1997; 36:339–354. [PubMed: 9096956]
34. Jay PY, Pham PA, Wong SA, Elson EL. A mechanical function of myosin II in cell motility. J Cell Sci. 1995; 108(Pt 1):387–393. [PubMed: 7738114]
35. Wilson CA, et al. Myosin II contributes to cell-scale actin network treadmilling through network disassembly. Nature. 2010; 465:373–377. [PubMed: 20485438]
36. Shulman Z, et al. Lymphocyte crawling and transendothelial migration require chemokine triggering of high-affinity LFA-1 integrin. Immunity. 2009; 30:384–396. [PubMed: 19268609]
37. Xu J, et al. Divergent signals and cytoskeletal assemblies regulate self-organizing polarity in neutrophils. Cell. 2003; 114:201–214. [PubMed: 12887922]
38. Dulyaninova NG, Malashkevich VN, Almo SC, Bresnick AR. Regulation of myosin-IIA assembly and Mts1 binding by heavy chain phosphorylation. Biochemistry. 2005; 44:6867–6876. [PubMed: 15865432]
39. Bullen A, Friedman RS, Krummel MF. Two-photon imaging of the immune system: a custom technology platform for high-speed, multicolor tissue imaging of immune responses. Curr Top Microbiol Immunol. 2009; 334:1–29. [PubMed: 19521679]
40. Kolega J. Phototoxicity and photoinactivation of blebbistatin in UV and visible light. Biochem Biophys Res Commun. 2004; 320:1020–1025. [PubMed: 15240150]

Author Manuscript Author Manuscript Author Manuscript Author Manuscript

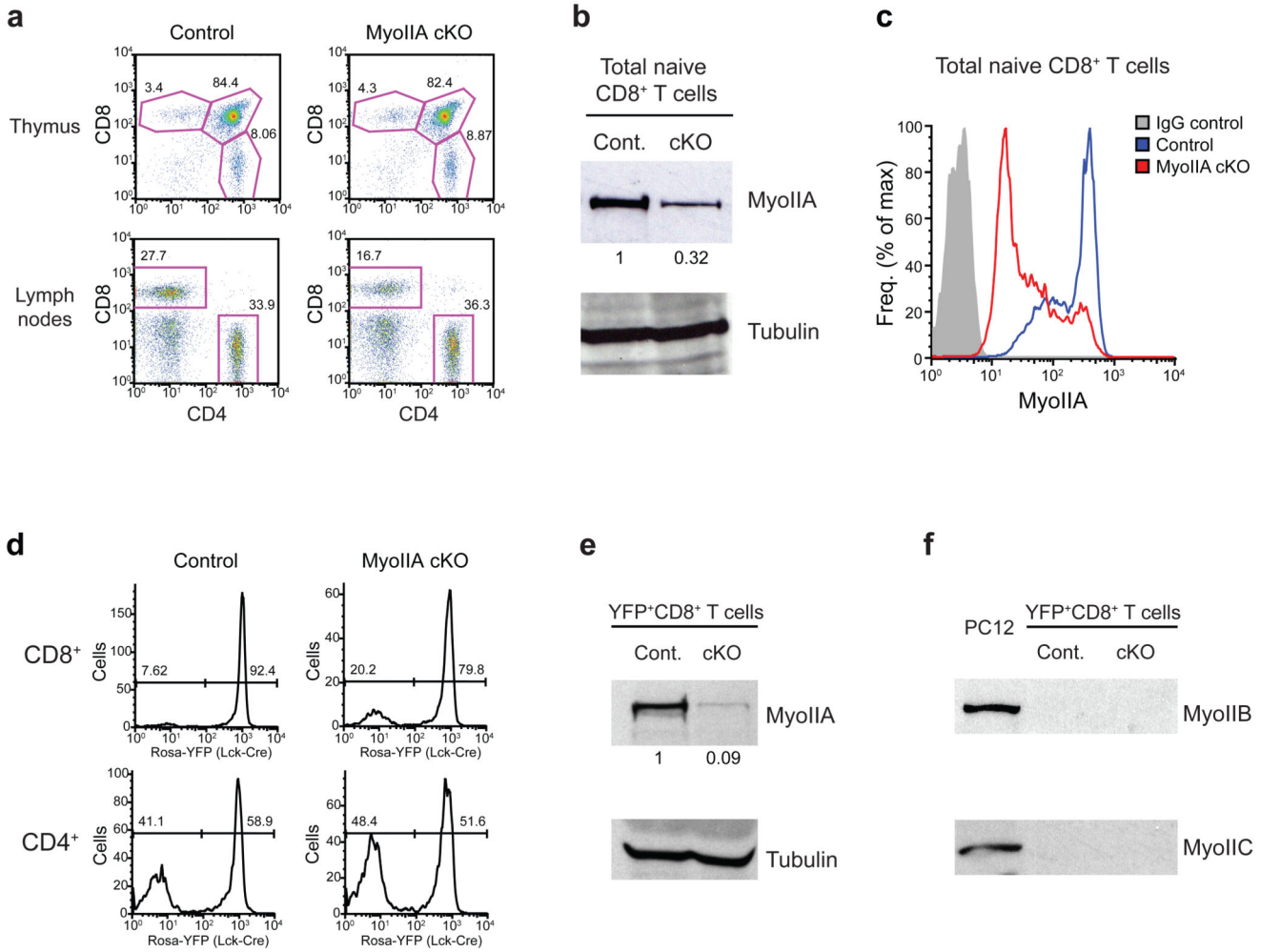

Figure 1. Depletion of MyoIIA in T cells from MyoIIA$^{flox/flox}$-Lck-Cre conditional knock-out mice

a) Representative FACS quantification of thymocyte development and peripheral naïve T cells from MyoIIA$^{wt/wt}$ (control) and MyoIIA$^{flox/flox}$ (MyoIIA cKO) mice expressing Lck-Cre. Three pairs of 5–9 week old age-matched mice were used for analysis of thymic development and 6 pairs of mice were used for peripheral T cell quantification. **b**) MyoIIA expression in peripheral naïve CD8$^+$ T cells from control and MyoIIA cKO mice. Expression was quantified by normalizing to tubulin. **c**) Control and MyoIIA cKO naïve CD8$^+$ T cells were fixed, permeabilized and stained for MyoIIA expression and analyzed by FACS. **d**) Frequency of Cre expression in mature single-positive CD8$^+$ and CD4$^+$ T cells in the lymph node determined using a Gt(Rosa26)Sor promoter-loxP-STOP-loxP-YFP (Rosa-YFP) transgenic reporter. **e**) MyoIIA expression in sorted YFP$^+$-CD8$^+$ peripheral T cells from MyoIIA$^{wt/wt}$/Lck-Cre$^+$/Rosa-YFP (control) and MyoIIA$^{flox/flox}$/Lck-Cre$^+$/Rosa-YFP (cKO) mice. Expression was quantified by normalizing to tubulin. **f**) Lack of Myosin-IIB and Myosin-IIC expression in sorted YFP$^+$-CD8$^+$ control and cKO peripheral T cells. The PC12 cell line was used as a positive control. All data are representative of three independent experiments.

Author Manuscript Author Manuscript Author Manuscript Author Manuscript

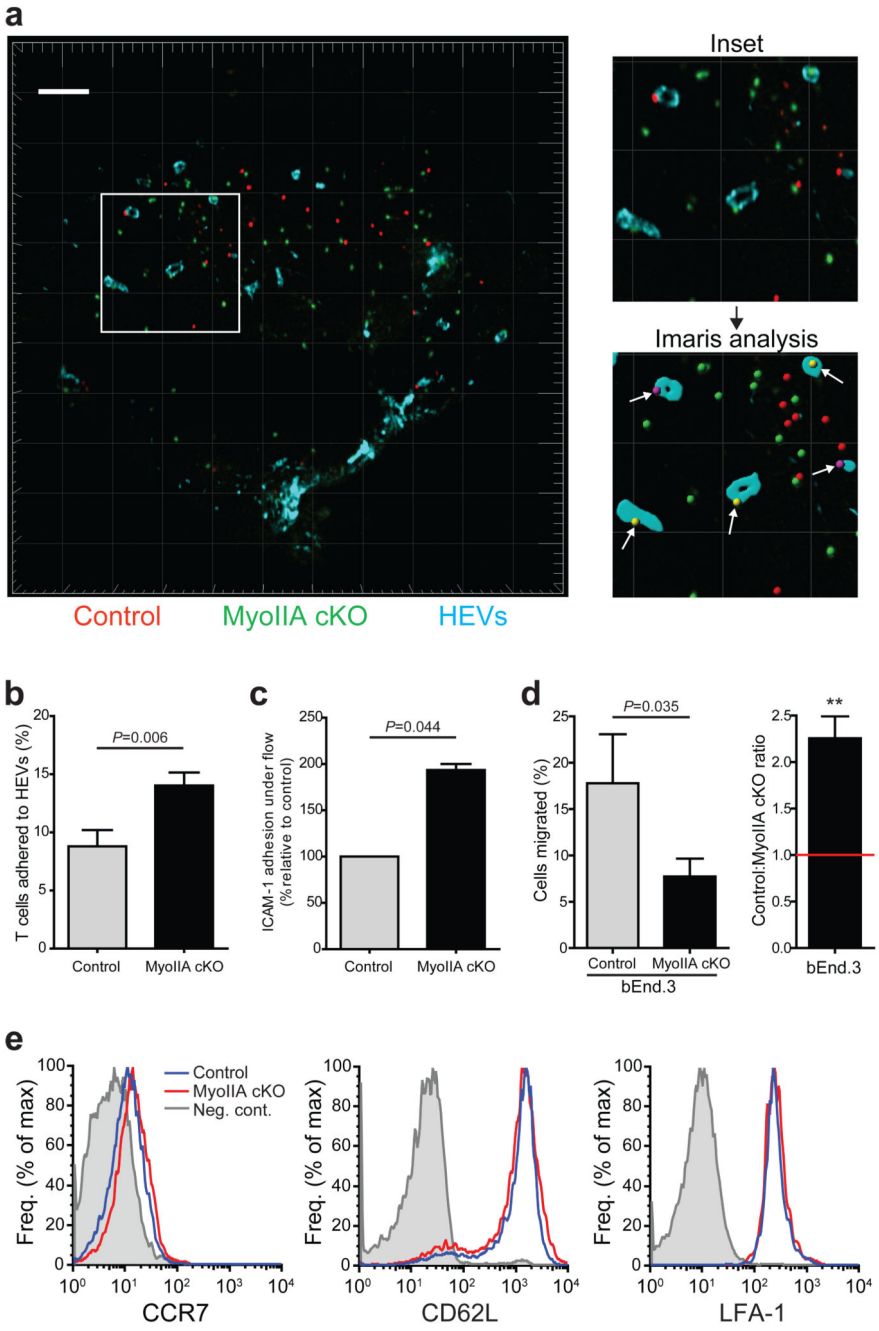

Figure 2. MyoIIA cKO T cells have increased contact with high endothelial venules and adhesion to integrin substrates

a) Representative cryosection of a popliteal lymph node harvested 2h after adoptive co-transfer of a 1:1 mix of fluorescently labeled control (red) and MyoIIA cKO (green) naïve $CD8^+$ T cells. Lymph node sections were stained with PNAd-1 antibodies to visualize high endothelial venules (HEVs) (blue). Top right panel, increased magnification of boxed area in left panel showing T cells in contact with HEVs. Bottom right panel, example of HEV surface rendering using Imaris software from the panel above and showing identification of

Author Manuscript Author Manuscript Author Manuscript Author Manuscript

cells in contact with HEVs (white arrows). White scale bar and light-grey grid intervals represent 100 μm. **b**) MyoIIA-deficient T cells have increased frequency of HEV contact during homing. The average percentage of control and MyoIIA cKO T cells found in contact with HEVs 2h after transfer was quantified. An average of 4 lymph node sections per experiment were analyzed with an ~50 cells for each group per lymph node section. **c**) Control and MyoIIA cKO $CD8^+$ T cells were injected into flow chambers and subjected to 10 min of physiological shear flow (2 dyne/cm^2); the number of adherent cells at the end time point was then quantified. **d**) Left panel, % trans-endothelial migration through a bEnd. 3 endothelial cell monolayer seeded on 5 μm pore transwells of control and MyoIIA cKO T cells in response to 1μg/ml CCL21. Right panel, ratio of control vs. MyoIIA cKO transmigrated T cells shown in the left panel. ** indicates $P<0.01$. **e**) Profile of CCR7, CD62L and LFA-1 expression of naïve $CD8^+$ T cells from control and MyoIIA cKO mice. Data in **a** and **e** are representative of three independent experiments; data in **b**–**d** are the averages (±SEM) from three independent experiments.

Author Manuscript Author Manuscript Author Manuscript Author Manuscript

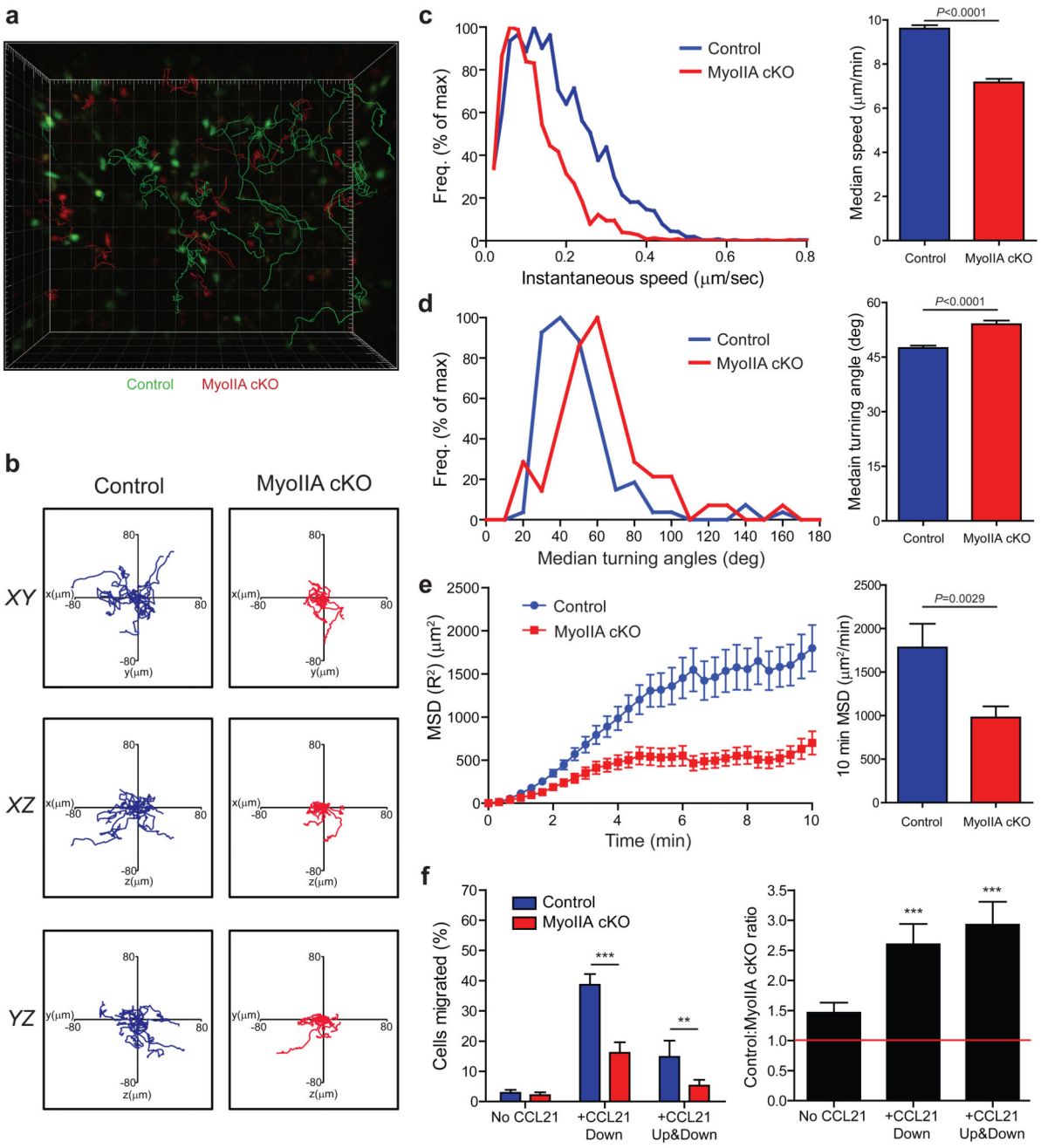

Figure 3. Naïve MyoIIA-deficient T cells have reduced intra-lymph node migration

Control and MyoIIA cKO naïve CD8$^+$ T cells were labeled and injected intravenously into recipient mice. Lymph nodes from recipient mice were then imaged by time-lapse 2-photon microscopy. **a**) Representative 3D reconstruction of a stage position with tracks overlaid. Control T cells in green and MyoIIA cKO in red; 20 randomly selected tracks are shown. **b**) Representative 10 min long tracks of 15 randomly chosen control and MyoIIA cKO T cells are shown. **c**) Representative distribution of instantaneous velocities (left panel) and average median velocity (±SEM) (right panel) of control and MyoIIA cKO T cells. **d**)

Author Manuscript Author Manuscript Author Manuscript Author Manuscript

Representative distribution of mean turning angles (left panel) and average median turning angle (±SEM) (right panel) of control and MyoIIA cKO T cells. **e**) Representative mean square displacements (MSD) (±SEM) over time (left panel) and average MSD over 10 min (right panel) of control and MyoIIA cKO T cells. **f**) Left panel, % migration (±SEM) of control and MyoIIA cKO naïve T cells in response to 1μg/ml CCL21 added to the bottom well (chemotaxis) or to both the top and bottom chambers of the transwell (chemokinesis). Right panel, ratio (±SEM) of control vs. MyoIIA cKO transmigrated T cells shown in the left panel. ** indicates $P<0.01$, and *** indicates $P<0.001$. Data in **a**, **b**, and left panels of **c**–**e** are from one stage position representative of three independent experiments. Data in **f** are averaged from three independent experiments; and right panels of **c**–**e** are pooled from multiple lymph nodes from each of three independent experiments.

Author Manuscript Author Manuscript Author Manuscript Author Manuscript

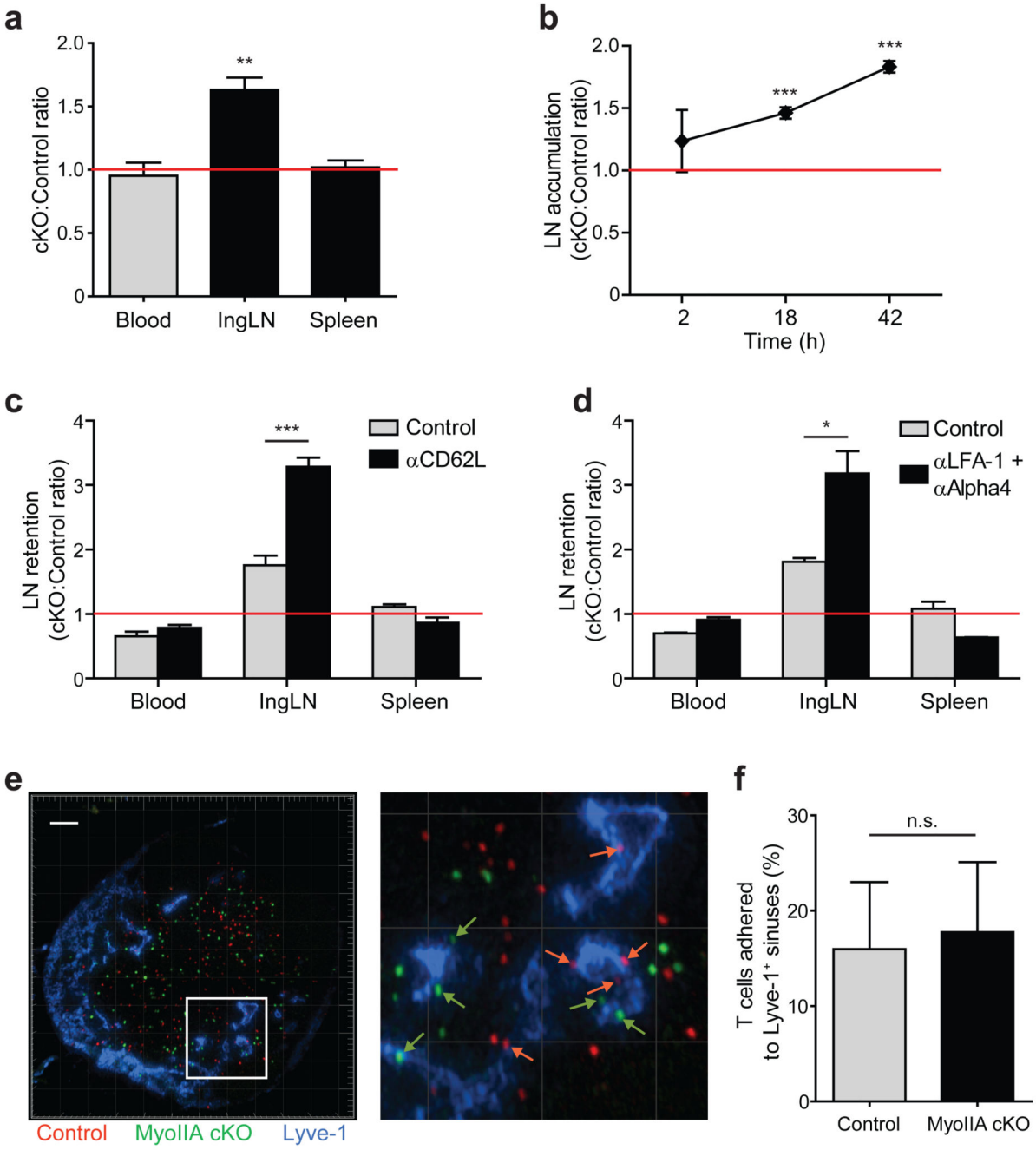

Figure 4. Naïve MyoIIA-deficient T cells have trafficking defects *in vivo* due to retention in the lymph nodes

a) MyoIIA-deficient T cells accumulate in lymph nodes of recipient mice over time. FACS quantification of the ratio of transferred MyoIIA cKO vs. control T cells in the blood, inguinal lymph nodes and spleen of recipient mice 18–42h post-transfer. The ratios for the lymph node and spleen are normalized to the ratio in the blood. **b**) Time course of accumulation of MyoIIA cKO T cells in the inguinal lymph node of recipient mice. The ratio of MyoIIA cKO vs. control T cells measured by FACS at 2, 18 and 42h post-transfer is

Author Manuscript Author Manuscript Author Manuscript Author Manuscript

shown. Data are normalized to the ratio in the blood. **c**) Lymph node retention of MyoIIA-deficient T cells. Ratios of transferred MyoIIA cKO vs. control T cells in the blood, inguinal lymph node (IngLN) and spleen 18h after treatment with PBS or anti-CD62L. **d**) Ratios of transferred MyoIIA cKO vs. control T cells in the blood, IngLN and spleen 18h after treatment with PBS or integrin-blocking antibodies. **e**) Representative cryosection of a popliteal lymph node harvested 42h after adoptive transfer of labeled control (red) and MyoIIA cKO (green) T cells. The lymph node sections were stained with Lyve-1 antibodies to visualize lymphatic endothelium (blue). Right panel, increased magnification of boxed area in left panel containing T cells in contact with the lymphatic endothelium (white arrows). White scale bar and light-grey grid intervals represent 100 μm. **f**) Quantification of the percentage of control and MyoIIA cKO T cells found in contact with lymphatic endothelium 42 hours after adoptive transfer. Multiple lymph node sections were analyzed with an average of 50 cells for each group per lymph node section. * indicates $P<0.05$, ** indicates $P<0.01$, and *** indicates $P<0.001$. Data in **a**–**c** are the average (±SEM) of at least four independent experiments. Data in **d** are the average (±SEM) of two independent experiments. Data in **e** and **f** are from three independent experiments.

Author Manuscript Author Manuscript Author Manuscript Author Manuscript

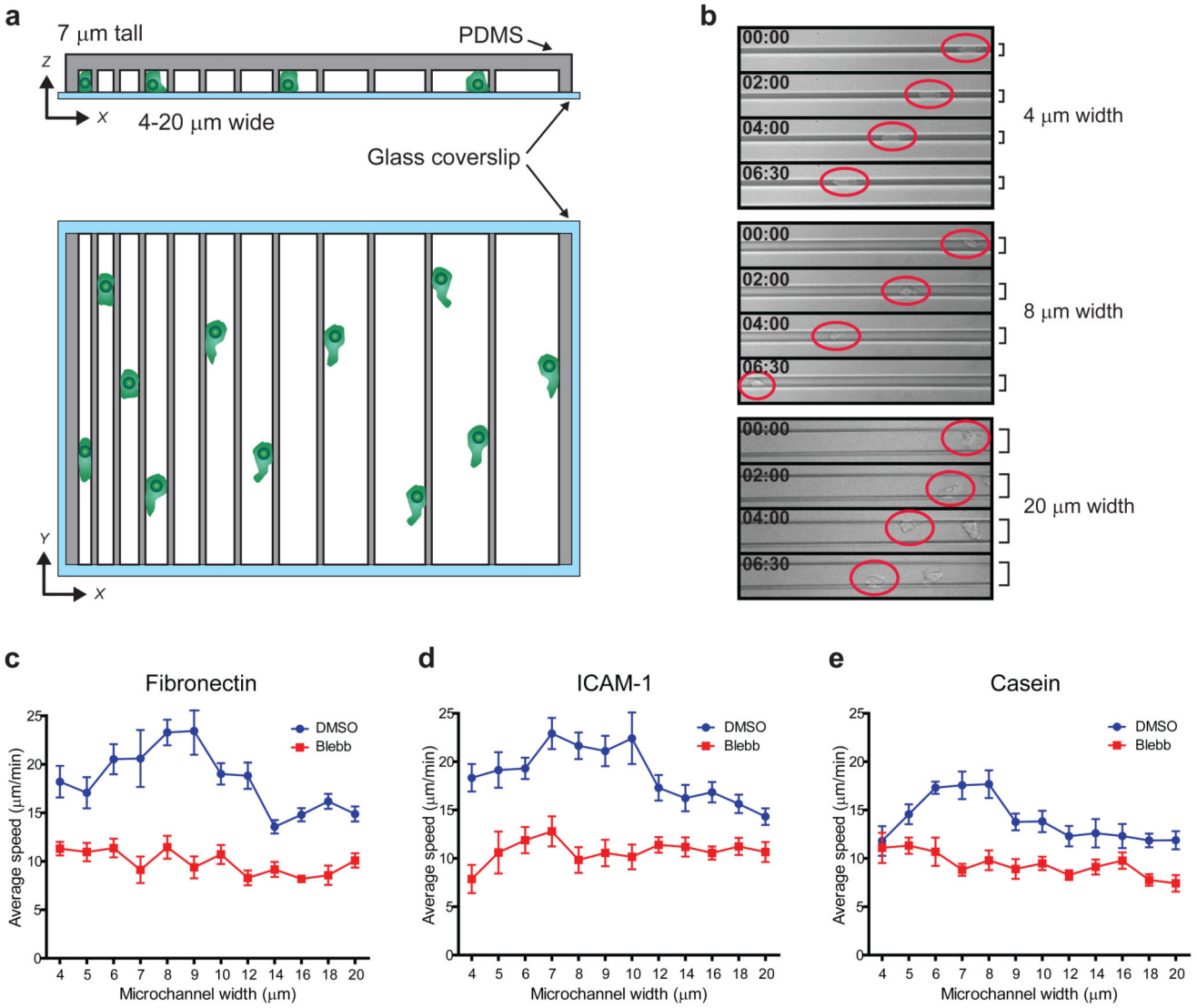

Figure 5. T cell migration efficiency within confined environments is controlled by MyoIIA

$CD8^+$ T cells 4–5 days post-activation were injected into micro-fabricated confining channels of variable size in the presence of vehicle control or 100 μM blebbistatin and then imaged. **a**) Schematic of variable microchannel array assembly. **b**) Representative examples of T cells crawling within microchannels of different width (as indicated) imaged by brightfield timelapse microscopy. Red circles highlight the position of the T cells; time is indicated in min:sec. **c**) Average speed (±SEM) shown as a function of microchannel size of control and blebbistatin treated T cells injected into fibronectin coated microchannels. **d**) Average speed (±SEM) shown as a function of microchannel size of control and blebbistatin treated T cells injected into ICAM-1 coated microchannels. **e**) Average speed (±SEM) shown as a function of microchannel size of control and blebbistatin treated T cells injected into casein coated microchannels. Data shown in **b** and **c** are representative of three independent experiments; data shown in **d** and **e** are representative of two independent experiments.

Author Manuscript Author Manuscript Author Manuscript Author Manuscript

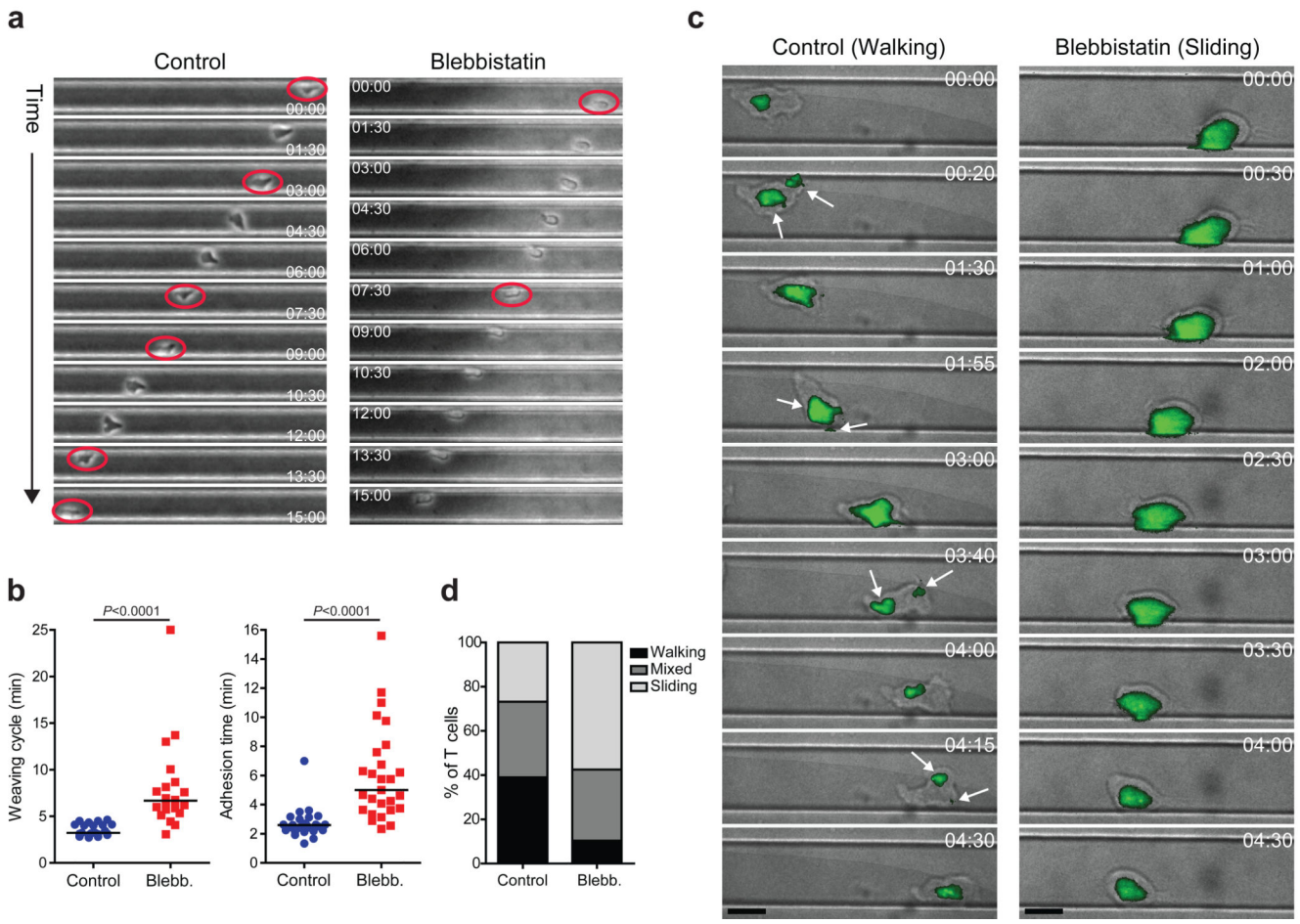

Figure 6. MyoIIA regulates T cell crawling mode under confinement

CD8$^+$ T cells 4–5 days post-activation were injected into fibronectin coated microchannels of variable size in the presence of vehicle control or 100 μM blebbistatin and then imaged. **a**) Representative 'weaving' behavior of control and blebbistatin treated cells migrating in 20 μm width channels. A control cell (left) and a blebbistatin treated cell (right) are shown over time at 1.5 min intervals. Red circles indicate the initial timepoint at which a cell has switched between microchannel walls. **b**) Left panel, median time interval of 'weaving' between walls of control and blebbistatin treated cells. Right panel, median duration of contact with a microchannel wall for control and blebbistatin treated cells in 18–20 μm width channels. **c**) Representative behavior of a 'walking' control T cell (left) and of a 'sliding' blebbistatin treated cell (right) migrating in microchannels over time. The brightfield images were overlaid with the TIRF adhesion area images (green). Brightfield and TIRF images were taken at 5 sec intervals for 5 min. CMTMR labeling of T cells enabled the TIRF read-out of adhesion areas without illuminating control and blebbistatin treated cells at wavelengths lower than 500 nm. White arrows in left panel highlight the presence of multiple distinct adhesion zones. Black scale bars represent 10 μm. **d**) Quantification of the frequency of the different crawling modes in microchannels of control and blebbistatin treated cells (P<0.0001; n>82 cells per treatment group). Data shown in **a**

and **b** are representative or pooled from three independent experiments. Data shown in **c** and **d** are representative or pooled from two independent experiments.

Author Manuscript Author Manuscript Author Manuscript Author Manuscript

Author Manuscript Author Manuscript Author Manuscript Author Manuscript

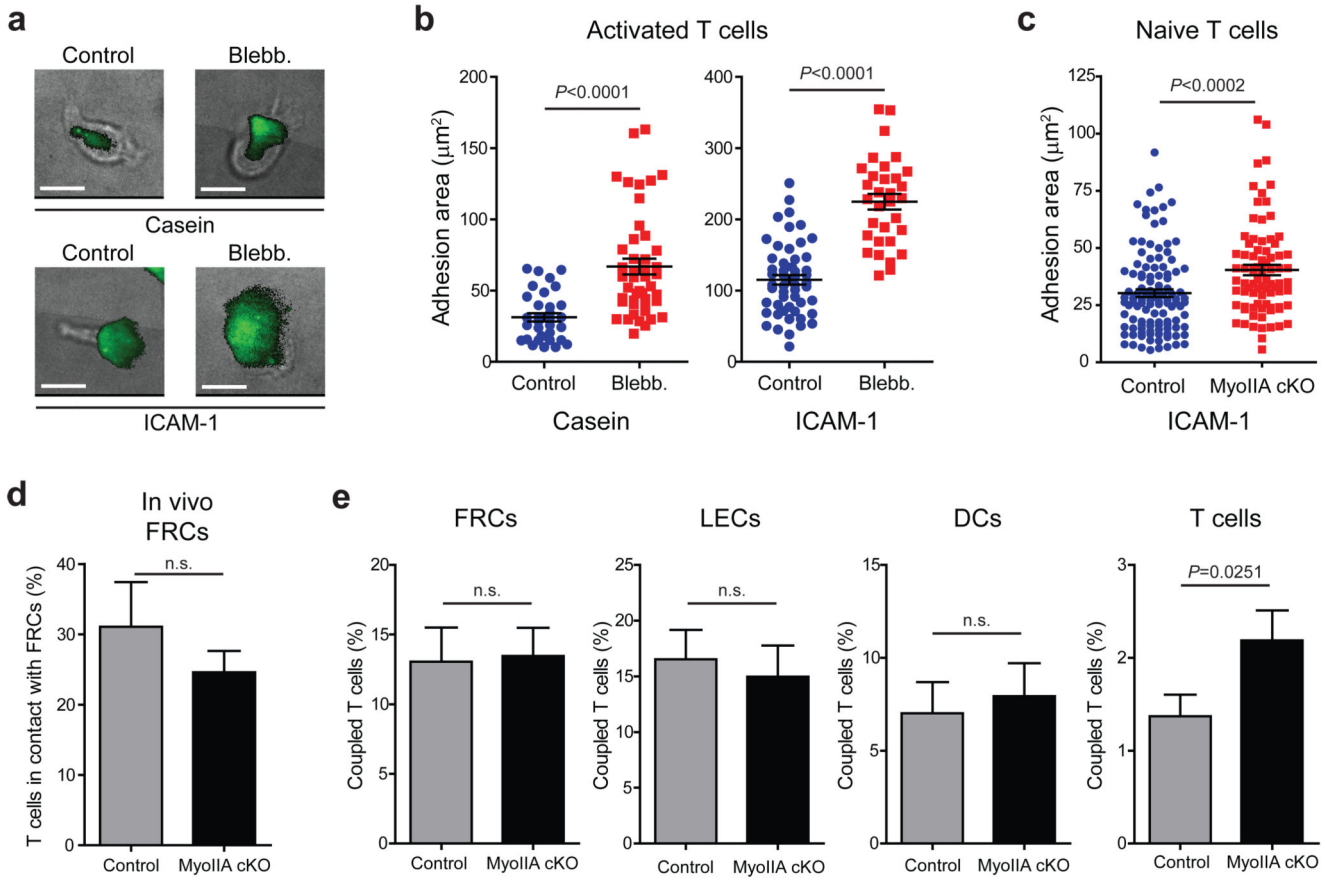

Figure 7. Deregulated surface adhesion of T cells lacking MyoIIA

a) Representative adhesion areas of control and blebbistatin treated $CD8^+$ activated T cells plated on glass coated with casein or ICAM-1. Overlays of the adhesion areas measured by TIRF microscopy (green) and of the brightfield channel are shown for each condition. White scale bars represent 10 μm. **b**) Quantification of the adhesion areas (±SEM) of control and blebbistatin-treated $CD8^+$ activated T cells on casein (left) or ICAM-1 (right). **c**) Quantification of the adhesion areas (±SEM) of control and MyoIIA cKO naïve $CD8^+$ T cells plated on ICAM-1. **d**) The percentage of transferred control and MyoIIA cKO naïve T cells in contact with the fibroblastic reticular cell (FRC) network in actin promoter-CFP chimeric mice was quantified by 2-photon microscopy. The average (±SEM) from multiple stage positions imaged from three independent experiments is shown. **e**) CFSE-labeled naïve $CD8^+$ T cells from control or MyoIIA cKO mice were mixed with CMTMR-labeled FRCs, lymphatic endothelial cells (LECs), dendritic cells (DCs), or naïve T cells as indicated. The average conjugation percentage (±SEM) of control and MyoIIA cKO T cells to each indicated cell type after 10 min incubation was quantified by FACS. Data from **a**–**c** are representative or pooled from at least two independent experiments; data from **d** and **e** are pooled from at least three independent experiments.